




Influential role of CdS film thickness in improving CdS/CdTe junction performance for solar cells: structural, optical, and electrical characterizations

Essam R. Shaaban^{1,*} , Mohamed A. Osman², Ali A. Osman², Marwa M. Sayed³, and Kamal I. Aly^{4,*}

¹ Physics Department, Faculty of Science, Al-Azhar University, Assiut 71542, Egypt

² Physics Department, Faculty of Science, Assiut University, Assiut 71516, Egypt

³ Chemistry Department, Faculty of Science, The New Valley University, El-Kharja 72511, Egypt

⁴ Chemistry Department, Faculty of Science, Assiut University, Assiut 71516, Egypt

Received: 11 August 2021

Accepted: 13 December 2021

Published online:
29 January 2022

© The Author(s), under exclusive licence to Springer Science+Business Media, LLC, part of Springer Nature 2021

ABSTRACT

CdS films of different thicknesses ($d \approx 100\text{--}300$ nm) are deposited on the glass substrate by thermal evaporation technique. The structure of these films had been studied by Rietveld refinement and atomic pressure microscope. The films of CdS/glass show a wurtzite type structure. XRD calculations show that the lattice parameters a and c have changed, the microstrain decreases, and the crystallite size increases. The optical constants refractive index n , and extinction coefficient, k consequently band gap are estimated from SE via construction an optical model. The refractive index n of the CdS/glass films received from SE model increases with growing of CdS layer thickness that is credited to the rise of the size of the crystal. It was also found that when the thickness of the CdS layer increases, the general behavior of the extinction coefficient k of the CdS/glass film increases. In addition, it is found that the direct optical transition with energy band gap is compact from 2.45 ($d = 100$ nm) eV to 2.25 eV ($d = 300$ nm). The Ni/n-CdSe/p-CdTe/Pt heterojunction has been assembled. The dark (cutting-edge-voltage) characteristics of fabricated heterojunctions had been suggested at the different thicknesses of CdS, as well as for voltages ranging from -2 to 2 V. Based on the dependence of the forward and reverse current at the voltage, the powerful and essential parameters related to the fabricated diode had been determined.

Address correspondence to E-mail: esam_ramadan2008@yahoo.com; Kamalaly@aun.edu.eg

1 Introduction

In the beyond few a long time, semiconductors have attracted fantastic attention. Among them, CdS is the most interesting because it has generated great interest in various applications of optoelectronics, photovoltaics, catalysis, and biological sensing [1–4]. CdS is n-type semiconductor and has an immediate optical energy gap of about 2.45 eV, which is usually recommended as a window sheet in solar cells. In addition to that CdS has a high photosensitivity and consequently performs an important position in provider production inside the solar cells [5, 6]. Structural and optical properties, making CdS a good candidate to be used as an insulating or buffer layer, are a prerequisite for a repeatable and efficient heterogeneous reaction in solar cells [7, 8]. Light absorption in the buffer layer (as an instance, band-gap energy, CdS = 2.4 eV) reduces the spectral response of the solar cell inside the blue region of the solar spectrum, because the photogenerated charge providers in the buffer layer are only in part accumulated. Analysis of polycrystalline thin-film solar cells identifies the absorption in the cadmium layer of the heterogeneous conduction as taking a large share in the total light loss [9, 10]. However, this loss due to light absorption is not the only consequence caused by the buffer layer. Many strategies were mentioned for the deposition of CdS thin films. These encompass thermal evaporation [11], sputtering [8], chemical bathtub deposition [12], spray pyrolysis [13], metal organic chemical vapor deposition (MOCVD) [14], molecular beam epitaxial approach [15], electro-deposition [16], photochemical deposition [17], and so forth. Among them, electron beam gun technique is a powerful technique for preparation of high-quality thin solid films. Therefore, on this research, the influence of CdS film thickness at the structural, morphological, and optical traits of CdS film has grown on glass substrates. The optical constant and the film thickness were decided with high accuracy in the basic segmentation spectroscopy (SE) strategies and software. The accurate values for optical constants, film thickness, and strength gap of the films are essential parameters in sun cells and photovoltaic packages. On the other hand, this framework pursuits to have a look at the dependence of darkish (I–V) characteristics in ahead and opposite bias at the film thickness and the voltage in the range of (– 2 to 2) volts.

2 Experimental details

High-purity (99.999%) CdS powder (Alrich chemical compounds organization, USA) became evaporated from molybdenum boat to form the dielectric layer onto ultrasonically cleaned glass substrate kept at regular temperature (150 °C), using a thermal evaporation unit (Denton Vacuum DV 502 A) and a vacuum of about 10^{-6} Pa. The substrate was circled at a gradual speed of five rpm to gain a uniform CdS thin film. The deposition rate and the film thickness had been controlled using a quartz crystal screen DTM-100. The deposition rate was maintained at 2 nm/s during evaporation of the films. The effect of film thickness on CdS has been studied at 5 different thicknesses (100, 150, 200, 250, and 300 nm). The films had been evaporated in a nitrogen environment to avoid any oxidation of the film. The constitution of the organized samples has been studied via XRD analysis (Philips X-ray diffractometry (1710)) with nickel filtered the radiation of Cu K α that has wavelength = 0.15418 nm). The XRD results had been delicate with the aid of the use of the Rietveld method with GSAS-II software [18, 19].

The composition analysis of the resulting film was performed by an (EDXS) unit (Philips XL), which was operated at an accelerating voltage of 30 kV. The error in determining the percentage of any element in the film does not exceed 2%. Atomic force microscope (AFM, model MLCT-MT-A) was used to analyze the morphology of the film surface.

Use the rotating compensator tool (J.A. Woollam, M-2000) to measure the SE parameters (ψ and Δ) of the CdS film in the wavelength range of 300–1100 nm. Ellipsometric statistics are performed at 70°. All measurements are performed at room temperature. The optical constants of the CdS films have been decided through fitting the version characteristic to the measured information the use of J.A. Woollam Corporation evolved WVASE32 program.

The heterojunction device of the Ni/n-CdS/p-CdTe/Pt solar cell was fabricated via deposition of the CdTe thin layer (500 nm) on the CdS thin films at five different thicknesses (100, 150, 200, 250, and 300 nm) which were deposited on pre-cleaned glass substrates. The front electrode contact was made by depositing a semi-transparent grid of platinum (Pt) fingers (100 nm) directly onto the surface of the CdTe thin layer, while the back contact electrode was attached to the CdS thin film deposited on the glass

substrates, which was nickel (Ni) and had a thickness of 100 nm. The front and back electrode contacts were considered ohmic for the small voltages. The current–voltage (*I*–*V*) measurements for the generated device were carried out using a standard circuit (Keithley 610 and 617 as a voltage source and current meter) to determine the current through the hetero-junction at various thicknesses of CdS. At room temperature, the dark (current–voltage) characteristics were obtained in a completely dark chamber,

3 Results

3.1 Structural characterization

Figure 1 illustrates the XRD pattern of CdS powder and the basic simulation test of Rietveld refinement using X’Pert HighScore (version 1.0e) software based on the CdS card. Therefore, the mirror image traces of the CdS powder are attributed to the hexagonal shape (wurtzite type, JCPDS 10-0454) [19–22].

Figure 2 displays the XRD of as-grown CdS thin film with various thicknesses on glass substrates. The treated samples showed a hexagonal CdS structure with crystal planes (100), (002), and (101). Regardless of the processing environment, as the crystallinity of the film increases, increasing the film thickness results in an increase in peak intensity [23].

Then, the crystal structures of the different thicknesses of the films were refined in terms of the

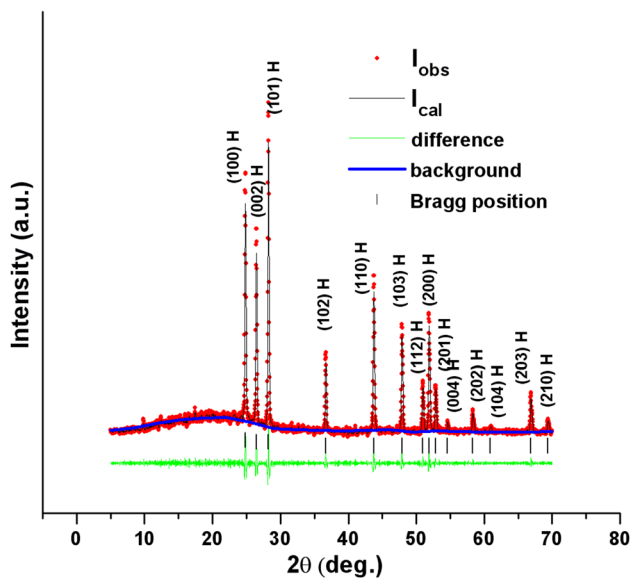


Fig. 1 XRD pattern of CdS powder with Rietveld Refinement

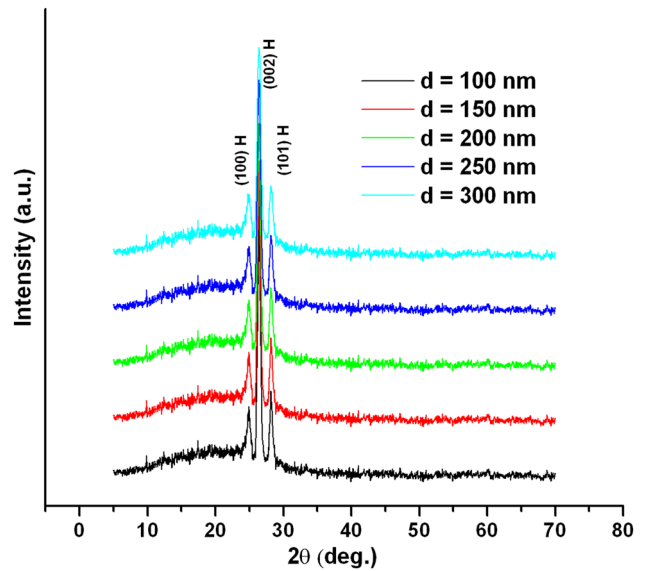


Fig. 2 X-ray diffractograms of the different thicknesses of CdS thin films

Rietveld method [18]. The Rietveld refinement results are presented as an examples in Fig. 3 (a, b, and c). The successful refinement is confirmed by the very small difference between the measured and refined intensities as revealed in Fig. 3 (a, b, and c) and the low *R*-factors scheduled in Table 1. According to the refined lattice parameters, as shown in Table 1, the lattice parameter is plotted in Fig. 4. As the film thickness grows, the lattice parameters *a* and *c* decrease.

XRD data were additionally analyzed to estimate the scale of crystallite, *D*, and microstrain, *e*, of the CdS film with exceptional thicknesses by way of the usage of the Scherrer and Wilson equations [11, 24, 25]. By analyzing XRD pattern in terms of Scherrer ($D = 0.9\lambda/\beta \cos \theta$) and Wilson equations ($e = \beta/4 \tan \theta$) equations [11, 24] crystallite size, *D*, and microstrain, *e* of as a function of film thickness of CdS could be identified after performing the correction ($\beta = \sqrt{\beta_{\text{obs}}^2 - \beta_{\text{std}}^2}$).

In which β is the broadening that equals the difference in profile width between the films β_{obs} and the standard (silicon) β_{std} .

The crystallographic properties were highly affected by the presence of dislocation density. The dislocation density is the dislocation lines number per unit area inside the thin film. The crystallite size, *D* is related to the dislocation density, δ by the relation ($\delta = 1/D^2$). The estimated values of crystallite size

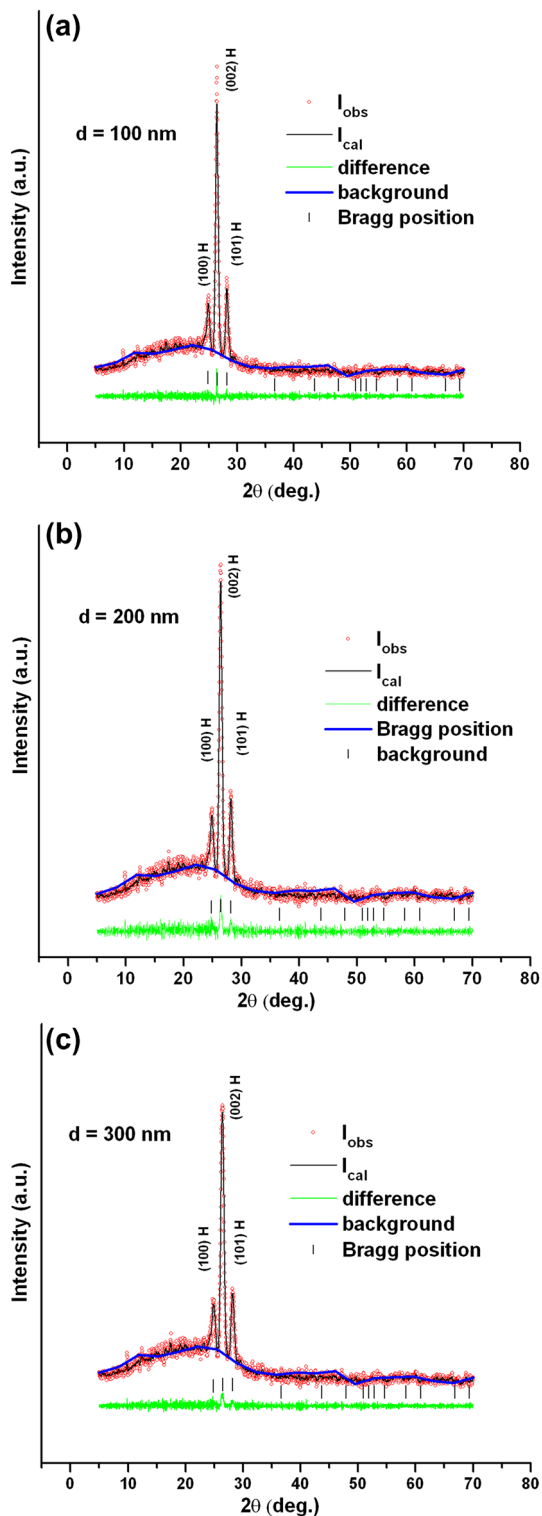


Fig. 3 X-ray diffractograms of the three thicknesses **a** 100 nm, **b** 200 nm, and **c** 300 nm of CdS thin films with Rietveld Refinement

and dislocation density as well as the values of microstrain are listed in Table 1. It is found that with increasing of the film thickness, the mean D of the CdS films increases, whereas the microstrain reduces (See Fig. 5). The increase in the crystallite size illustrates a reduction of the dislocation density and crystal imperfections within the lattice, thereby reducing internal microstrain. To probable clarify this behavior, higher thickness of the film may additionally mean a better compact stresses in the equivalent film, which can also suggest a much fewer efficient tensile stress and/or strain during the manner of the granule growth, as a result, leading to a larger grain size. The consequences of thickness dependent of ZnS (that comparable of CdS) thin films are in accord with the ones given by using another agencies [26–28].

AFM studies have been used to microscopically describe the surface morphology of CdS films with different thicknesses. Figure 6 shows 3-dimensional (3D) AFM images of 100, 200, and 300 nm films. The picture shows that the surface of the film is clearly dense and evenly arranged. The oriented normal distribution of the elongated grains has similar guidelines, confirming that the positioned favorable orientation grains grow toward the (002) plane. The micrographs of CdS films of different thicknesses were analyzed in detail to determine the microscopic surface morphology parameters, including grain length, surface roughness, and root implied rectangular (RMS) surface roughness, as shown in Table 1. The facts indicate that the grain size will increase with increasing film thickness. However, it was found that the inside roughness and RMS surface roughness increase with the thickness growth.

3.2 Optical properties in terms of spectroscopic ellipsometric

Semiconductor skinny films have many crucial technical programs, along with optoelectronic device. The presentation of CdS films in large part relies upon on their optical residences and thickness. Spectroscopic ellipsometry (SE) has been used to identify the optical constants precisely. The SE is non-damaging optical strategies and uses layer model to achieve an outcome results.

The spectroscopic ellipsometric outcomes of CdS films evaporated on transparent glass measured by way of SE method are changed into within the

Table 1 Values of lattice parameters (*a* and *c*), volume of unit cell, crystallize size, lattice strain, dislocation density, surface roughness, and RMS surface roughness of different thicknesses of CdS thin films

Thick (nm)	<i>a</i> = <i>b</i> (Å)	<i>c</i> (Å)	<i>V</i> (Å ³)	<i>R</i> -factor	Cry. Size (nm)	Lattice Str × 10 ⁻³	Disloc. density × 10 ⁻⁴ (lines/nm ²)	Surface roughness (nm)	RMS Surface roughness (nm)
100	3.895	6.399	102.354	3.22	16	3.95	38	1.526	0.981
150	3.894	6.397	102.240	3.41	19	3.89	28	1.761	1.186
200	3.89	6.387	101.956	3.56	23	3.76	19	2.552	2.384
250	3.886	6.382	101.672	3.67	25	3.56	15	3.066	2.434
300	3.885	6.38	101.559	3.75	27	3.34	14	3.626	2.972

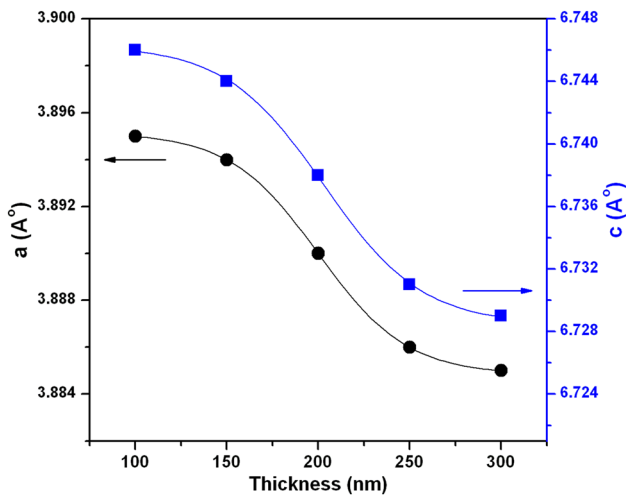


Fig. 4 Lattice parameters *a* and *c* of a wurtzite CdS films that extracted from Rietveld Refinement

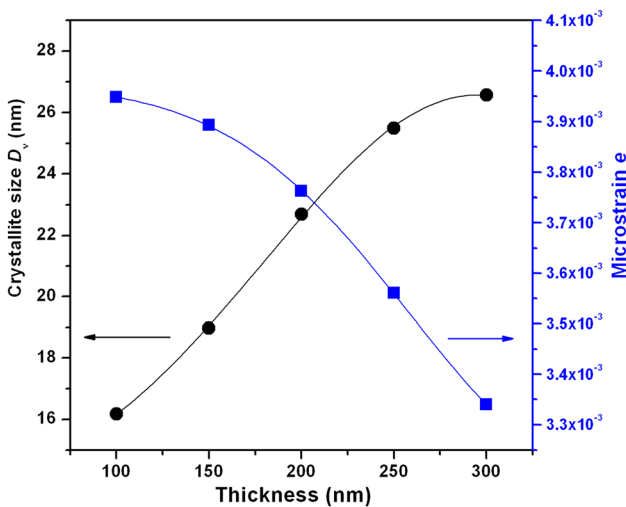


Fig. 5 Crystallite size and lattice strain of CdS nanofilms

spectral variety of 300–1100 nm at an prevalence angle of 70°, and the information is amassed in intervals of 5 nm. The confused mirrored image is eliminated through the use of roughen substrate backs. Spectroscopic ellipsometry without delay information angles Ψ and Δ , which can be connected to the complex mirrored or reflected image coefficients (Fresnel’s coefficient) of the polarized light by the subsequent equation [27–30]:

$$\rho = \frac{r_p}{r_s} = \tan \psi \exp(i\Delta), \tag{1}$$

wherein Ψ , Δ , r_p , and r_s are mentioned the angle received from the amplitude ratio among the parallel polarized wave (*p*) and perpendicularly polarized wave (*s*), the polarized waves exchange. The Spectral ellipsometric facts ψ_{exp} and Δ_{exp} of CdS/glass films among outcomes of CdS thickness are provided in Fig. 7. The optical values of *n*, *k*, and *d* of the CdS films are determined by using least-squares regression evaluation and mean square error function (MSE) to change the spectral dependence of ψ_{exp} and Δ_{exp} into the correct version to obtain unidentified fitting parameters with high precision. The Levenberg–Marquardt regression rule set is completely based on the record-matching estimation and the modeling facts of ψ and Δ , and is used to reduce MSE and select the effectiveness of subsequent versions [31, 32]:

$$\text{MSE} = \frac{1}{2N - M} \sum_{i=1}^N \left(\left(\frac{\psi_i^{\text{mod}} - \psi_i^{\text{exp}}}{\sigma_{\psi,i}^{\text{exp}}} \right)^2 + \left(\frac{\Delta_i^{\text{mod}} - \Delta_i^{\text{exp}}}{\sigma_{\Delta,i}^{\text{exp}}} \right)^2 \right) \tag{2}$$

in which *M* is the appropriate parameters range and *N* is the number of ψ_{exp} and Δ_{exp} pairs included in the fitting, and that *i* is the index of summation. The

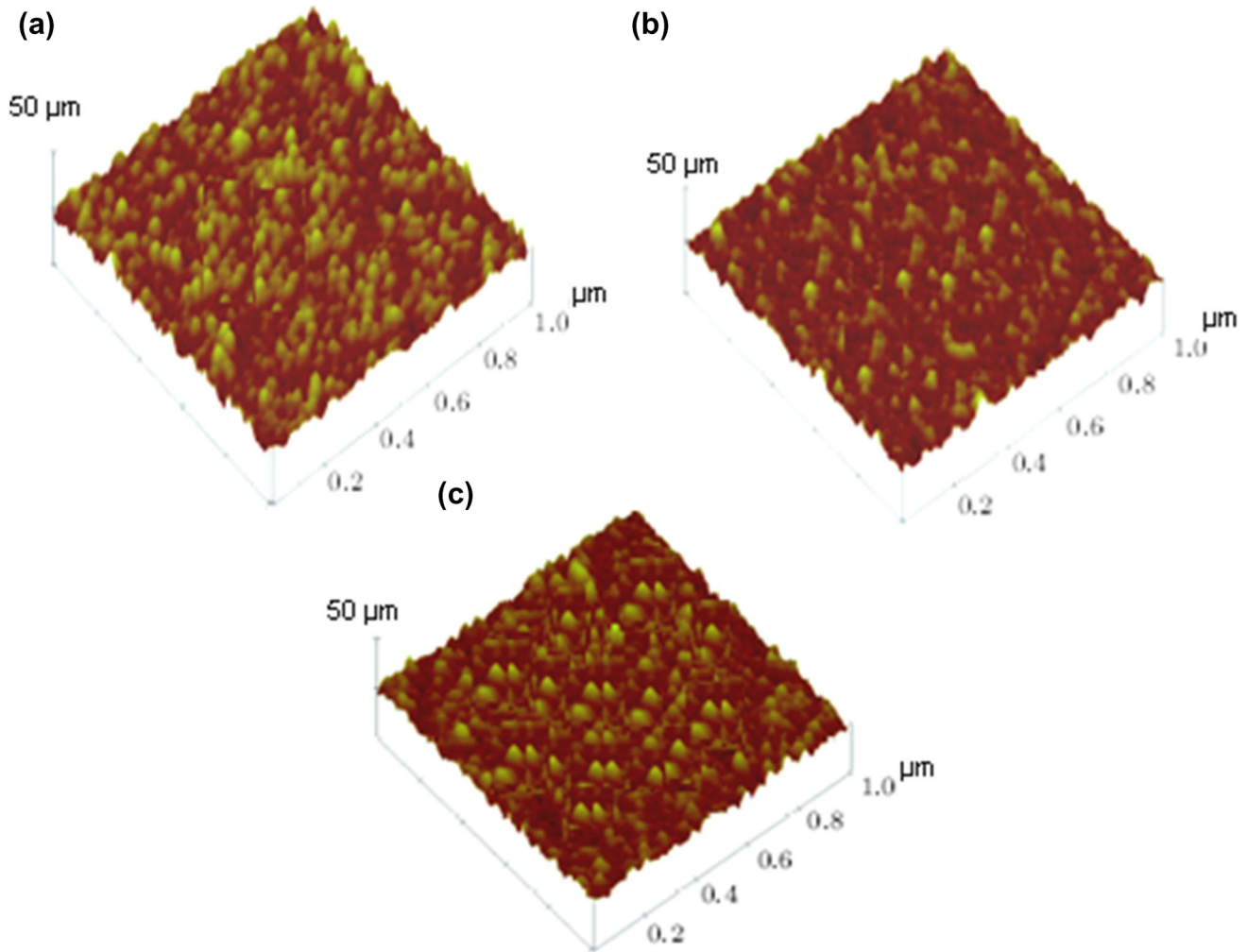


Fig. 6 AFM images of CdS thin films deposited at thicknesses **a** 100 nm, **b** 200 nm, and **c** 300 nm

values of ψ_i^{exp} , Δ_i^{exp} , and ψ_i^{mod} , Δ_i^{mod} are called the measured and modeled values, respectively. $\sigma_{\psi_i}^{\text{exp}}$ and $\sigma_{\Delta_i}^{\text{exp}}$ are the standard deviations of ψ_i^{exp} and Δ_i^{exp} , respectively.

Use the Complete Ease SE software program to use the appropriate optical model to evaluate the SE parameters through nonlinear regression coefficients [33]. In the existing examine, the model is built to provide a stacked-layer shape, that is particularly composed of 3 layers: a pitcher substrate, CdS absorber layer, and a rough layer. The rough layer is modeled by using the effective medium approximation (EMA) that is the suitable device to establish the morphology of the multilayer film configuration. More details about EMA are available and described in index [34]. Besides, the glass layer is modeled by using Cauchy version belt in Complete EASE

software, while the CdS layer is modeled with the aid of the usage of the B-spline computational process. The B-splines are a recursive set of polynomial splines. More details about polynomial splines are noted in details in ref. [28]. Figure 8a, b shows the spectral changes of ψ_{exp} and Δ_{exp} of CdS/glass of 100 and 300 nm CdS layer thicknesses, respectively), which are suited to the calculated ψ_i^{cal} and Δ_i^{cal} data received using the above recommended model. As the thickness of the CdS layer increased from 100 to 300 nm, the fitting process produced a very low MSE value, from 1.17 to 1.77, and the surface roughness of the CdS film increased from 1.66 nm to 3.76 nm. In addition, the interference pattern in the spectrum is caused by the coherence of a pair of reflections in the film [35]. The fitted optical constants, namely the refractive index, n and extinction coefficient, k of CdS

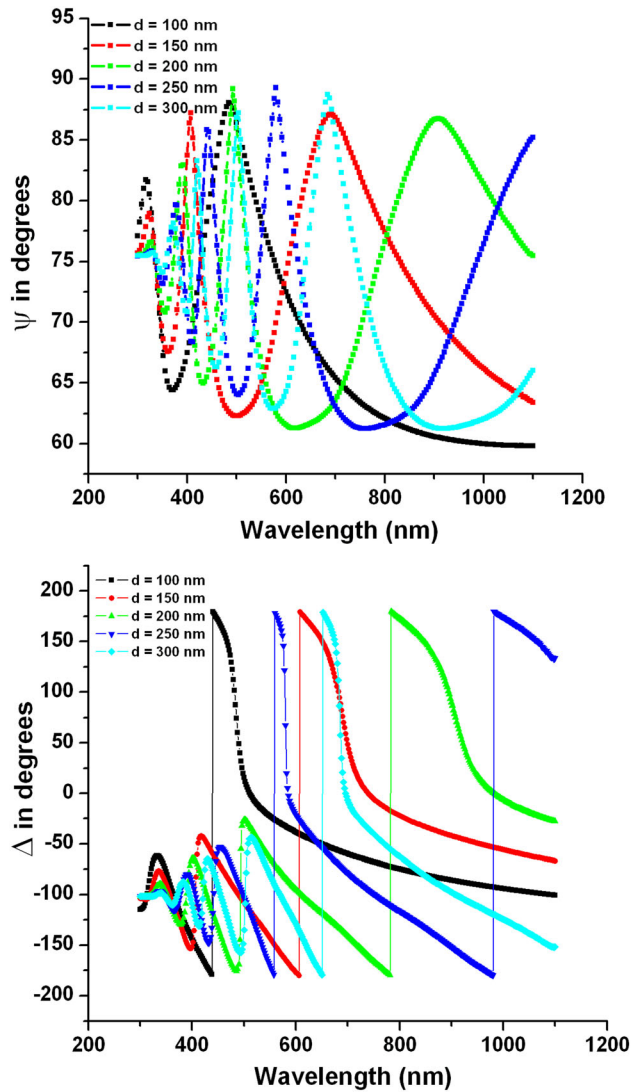


Fig. 7 Spectral ellipsometric data ψ and Δ for various thicknesses of CdS thin films grown on glass substrate

films with different thicknesses, are shown in Figs. 9 and 10, respectively.

In addition, it was observed that the refractive index increased with the increase of the thickness of the CdS layer, which was attributed to the enhance in crystallinity, which led to the enhance in grain size [36]. Figure 9 shows the k spectral behavior of CdS/glass films with various CdS layer thicknesses obtained from the above model. Obviously, a significantly lower extinction coefficient is observed at the absorption edge, which confirms that the light is absolutely stopped in this variety [37].

The absorption coefficient (α) of CdS/glass films with diverse CdS layer thicknesses was calculated in

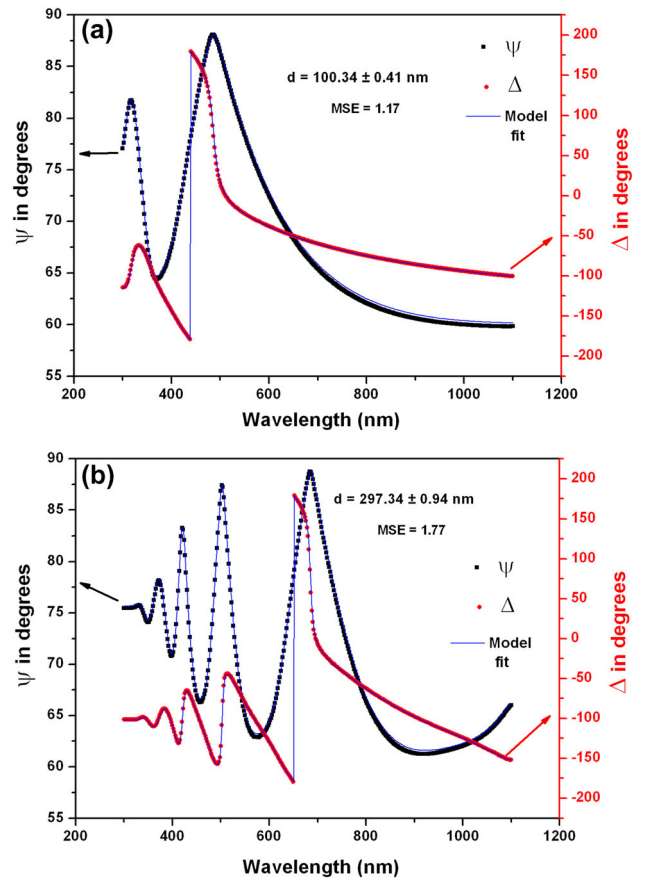


Fig. 8 Spectral ellipsometric data ψ and Δ for **a** 100 nm and **b** 300 nm for CdS thin films.grown on glass substrate. Experimental results are indicated by symbols, and the solid lines represent the model fit data

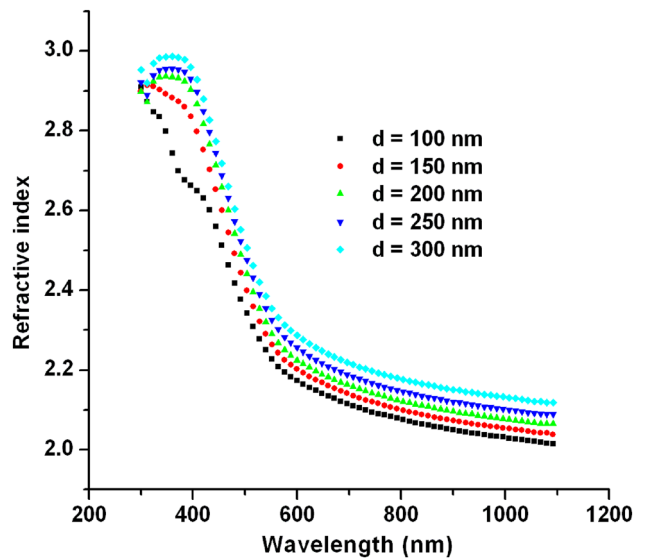


Fig. 9 Dispersion refractive index for CdS with different thicknesses

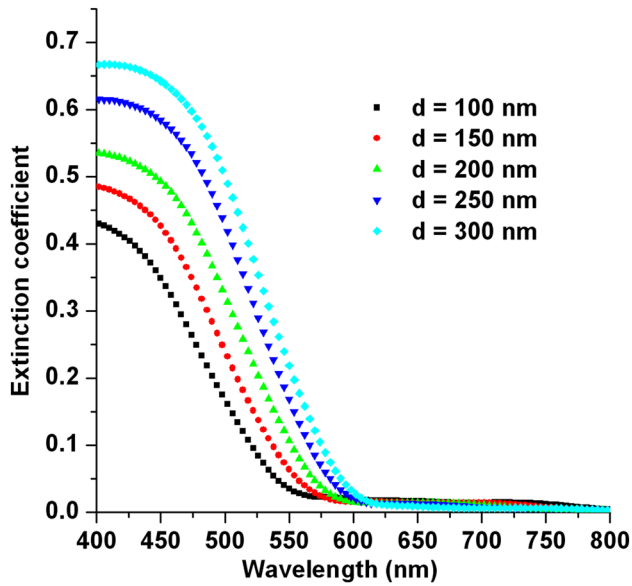


Fig. 10 Extinction coefficient against wavelength for CdS with different thicknesses

terms of k value that extracted from SE model via the subsequent relation [38]:

$$\alpha = \frac{4\pi k}{\lambda}. \quad (3)$$

Figure 11 shows the relationship between α and $h\nu$ for CdS/glass films with extraordinary CdS layer thickness. As well the absorption behavior increases

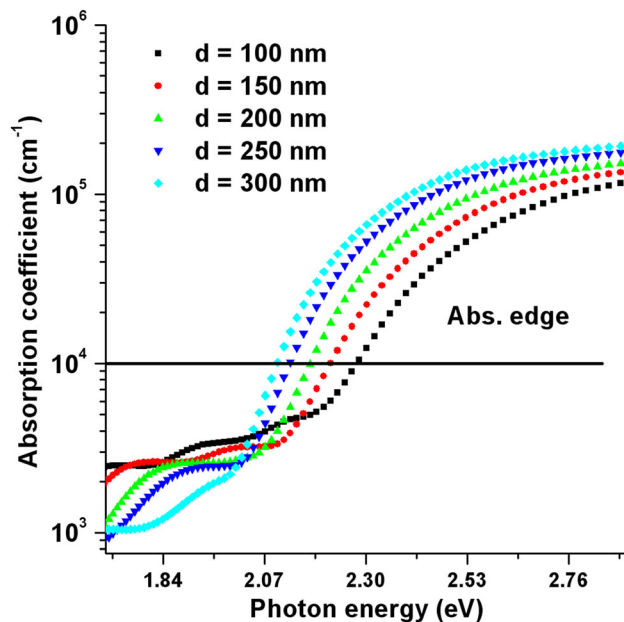


Fig. 11 Absorption coefficient against photon energy for CdS with different thicknesses

as the thickness of the CdS layer increases, especially in the UV range [39]. In addition, the non-zero value of light absorption observed at energies less than the original absorption edge is owing to light absorption at the grain boundaries [40, 41].

At strong absorption region, where $\alpha > 10^4 \text{ cm}^{-1}$, The optical energy band gap E_g^{opt} of varies thicknesses of CdS can be calculated using the Tauc relation of the following expression that can be used [42]:

$$(\alpha h\nu) = \alpha_o (h\nu - E_g)^p, \quad (4)$$

where α_o and p are constant and exponent. Equation 4 is the one that determines the type of optical transformations, whether they are allowed or not, depending on the p value. Since the CdS film is polycrystalline, as shown by X-ray diffraction, the transition will most likely be permissible, i.e., a p value of half ($p = 1/2$) [43–46]. Figure 12 shows the relationship of $(\alpha h\nu)^2$ on the vertical axis with $h\nu$ on the horizontal axis of different thicknesses of CdS layer. The value of the gap energy, E_g^{opt} is determined by extending the line part of $(\alpha h\nu)^2$ to cut the horizontal axis, $h\nu$ at a zero value of $(\alpha h\nu)^2$, which is the value of the gap energy. Figure 13 shows the energy gap, E_g^{opt} values as a function of CdS film thickness. It is observed that the value of E_g^{opt} of CdS film decreases as the thickness of the CdS layer increases. Various information have been published to explain that the band gap decreases with the increase of semiconductor film thickness, such as the quantum

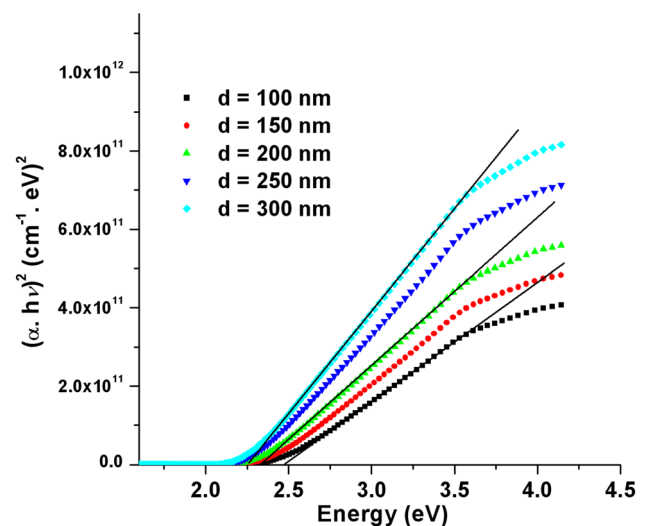


Fig. 12 Variations of $(\alpha h\nu)^2$ versus photon energy ($h\nu$) for CdS films with different thicknesses

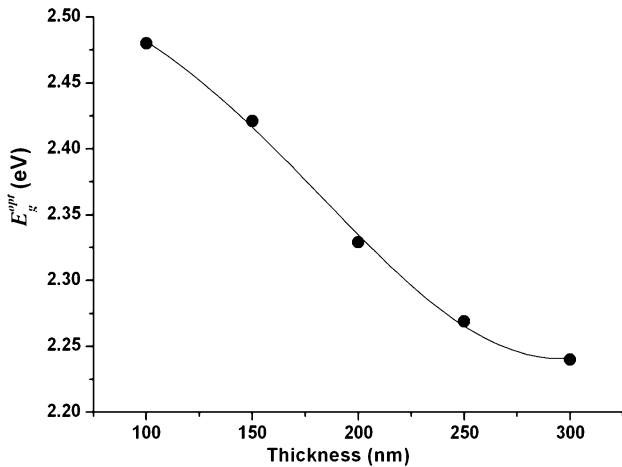


Fig. 13 Optical energy gap, E_g^{opt} as a function of CdS film thickness

size effect [47, 48], structural parameters [49], the appearance of impurities [50, 51], and the reduction of stress and potential density of dislocations [52, 53]. In this study, the observed decrease in the optical E_g^{opt} of CdS/glass films with the increase in CdS layer thickness is attributed to structural and microstructural parameters, e.g., increment in particle size, the reduction in lattice parameters, and lattice microstrain. In this study, the observed decrease of E_g^{opt} for CdS/glass films with increasing thickness of CdS layer is attributed to change in microstructures, e.g., diminish in lattice parameters, enlarge in crystallize size, and fine lattice compaction.

3.3 Photovoltaic characteristics for fabricated solar cell

The main parameters of the fabricated solar cells are extracted in this work in the temperature range of 100 to 300 nm to determine the behavior of dark ($I-V$) characteristics for the forward and reverse bias applied in the range of -2 to 2 V. The diagram of studied p–n junction is illustrated in Fig. 14.

The current I is related to the applied voltage V and the rest of the parameters of the fabricated diode is the following famous equation [54]:

$$I = I_{01} \left(\exp \left(\frac{q(V - IR_s)}{n_1 k_B T} \right) - 1 \right) + I_{02} \left(\exp \left(\frac{q(V - IR_s)}{n_2 k_B T} \right) - 1 \right) + \left(\frac{V - IR_s}{R_{sh}} \right). \quad (5)$$

In this formula, I_0 symbolizes the saturation current, n epitomizes the quality factor of the fabricated

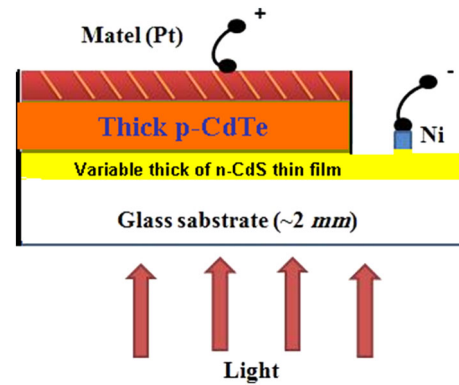


Fig. 14 The diagram of studied p–n junction n-CdS/p-CdTe Cell

diode), q is the electronic charge which is equal to $(1.6 \times 10^{-19} \text{ C})$ and k_B recaps the Boltzmann constant. The rest parameters in Eq. (5) represent the parasitic resistances which include the shunt resistance R_{sh} and series resistance R_s .

3.4 The pathway of (current–voltage) dependence

Figure 15 depicts the dark ($I-V$) features for the manufactured diode in forward and reverse bias for the variable thickness of CdS and applied voltage in the specified ranges. It will be clear from this figure that the current increases as the thickness of the film increases. Figure 16 shows the dependence of the current on the applied voltage in the forward bias and reverse bias to highlight the success of the

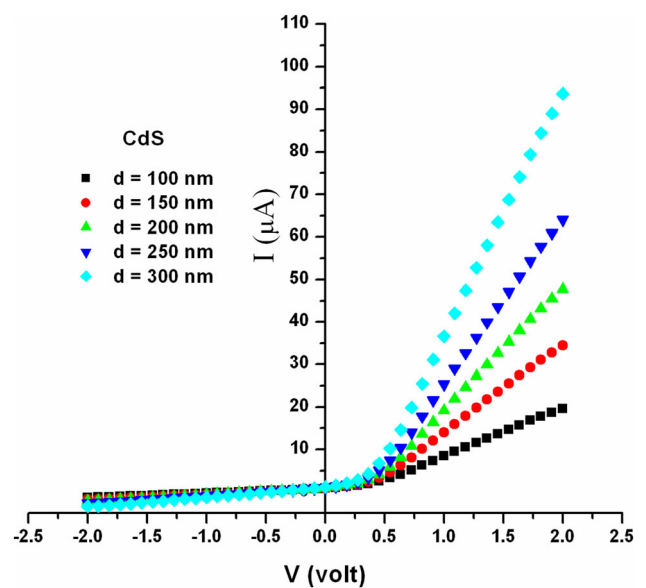


Fig. 15 The dark ($I-V$) characteristics for the fabricated solar cell

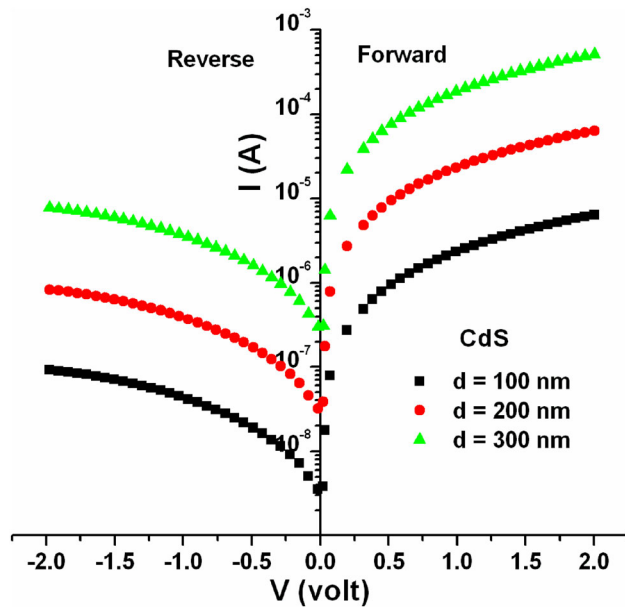


Fig. 16 Current versus the applied voltage for the p–n junction of solar cell at various thicknesses of CdS in the range of (– 2, 2) volts

studied solar cell synthesis with high efficiency so that the current in the forward bias is higher than the current in the reverse bias (I – V). These graphs depict the increase in the current behavior of the generated solar cell in the case of the forward bias, which increases dramatically in the low-voltage region. The development and formation of a depletion (exhaustion) region between the CdS thin film formed on the glass substrate and the CdTe thin film deposited on it are related to the exponential behavior in the low voltages. It should be observed that the exponential behavior of the reverse current of the examined manufactured solar cell in the depletion zone, i.e., in the low-voltage region, is lower than the exponential behavior of the forward current in the same region. As a result, the fabricated solar cell can be said to have exceptional rectification characteristics.

4 Conclusions

CdS films with diverse thicknesses (100–300 nm) are deposited on the glass substrates (CdS/glass) by evaporation. The influence of thickness on optical traits of the (CdS/glass) is considered with the aid of usage spectroscopic ellipsometric (SE). The structural examination tells that CdS/glass film includes a wurtzite hexagonal CdS film form structure. It is

discovered that as the CdS film thickness increases, lattice constants and strain decrease, even as the crystallites size increases. The consequences received from SE display that the general behavior of the optical constants, n and k for the CdS/glass film increases with the raise of CdS layer thickness. The outcomes in addition display that the E_g^{opt} with direct nature reduces as the thickness increases from 100 to 300 nm. It is accomplished that the optical constants of CdS films enhance, as the CdS film thickness increases. Furthermore, it is discovered that the deposition of CdS glass substrate increased absorption with increase in the film thickness and then reduced the band gap. On the other hand, the constructed solar cell's forward and reverse biases have been thoroughly analyzed. In the case of forward bias, the current behavior of the generated solar cell increases, which increases significantly in the low-voltage region. The development and formation of the depletion (depletion) region between the CdS film formed on the glass substrate and the CdTe film deposited thereon is related to the exponential behavior at low voltage.

Acknowledgements

This work was produced with the financial support of the Academy of Scientific Research and Technology of Egypt; ScienceUP/GradeUP initiative: Grant Agreement No (6505). Its contents are the sole responsibility of the authors and do not necessarily reflect the views of the Academy of Scientific Research and Technology.

Author contributions

ERS: Conceptualization, investigation, calculations, writing—original draft. MAO: Investigation and contribution to writing. AAO: investigation and editing. MMS: Investigation and taking measurements. KIA: Supervising and writing—reviewing and editing.

Data availability

Data supporting the findings of this study are available from the authors upon reasonable request at any

time. Research data policy It is easy for researchers participating in this research to share data and files that support their publications and give them to any recognized research center or scientific institution that wants these results.

Declarations

This research is in real compliance with ethical standards, because none of the results obtained by the research team contradicts any previously published results.

Conflict of interest The authors declare that they have no known competing scientific, financial, or personal interests in relationships that could appear to influence the work described in this paper.

References

- J. Han, C. Spanheimer, G. Haindl, G. Fu, V. Krishnakumar, J. Schaffner, C. Fan, K. Zhao, A. Klein, W. Jaegermann, Optimized chemical bath deposited CdS layers for the improvement of CdTe solar cells. *Sol. Energy Mater. Sol. Cells* **95**, 816–820 (2011). <https://doi.org/10.1016/j.solmat.2010.10.027>
- B. Ullrich, J. Tomm, N. Dushkina, Y. Tomm, H. Sakai, Y. Segawa, Photoelectric dichroism of oriented thin film CdS fabricated by pulsed-laser deposition. *Solid State Commun.* **116**, 33–35 (2000). [https://doi.org/10.1016/S0038-1098\(00\)0267-2](https://doi.org/10.1016/S0038-1098(00)0267-2)
- R.K. Sharma, K. Jain, A.C. Rastogi, Growth of CdS and CdTe thin films for the fabrication of n-CdS/p-CdTe solar cell. *Curr. Appl. Phys.* **3**, 199–204 (2003). [https://doi.org/10.1016/S1567-1739\(02\)00201-8](https://doi.org/10.1016/S1567-1739(02)00201-8)
- X. Mathew, J.P. Enriquez, A. Romeo, A.N. Tiwari, CdTe/CdS solar cells on flexible substrates. *Sol. Energy* **77**, 831–838 (2004). <https://doi.org/10.1016/j.solener.2004.06.020>
- N. Amin, K. Sopian, M. Konagai, Numerical modeling of CdS/CdTe and CdS/CdTe/ZnTe solar cells as a function of CdTe thickness. *Sol. Energy Mater. Sol. Cells.* **91**, 1202–1208 (2007). <https://doi.org/10.1016/j.solmat.2007.04.006>
- H. Kim, D. Kim, Influence of CdS heat treatment on the microstructure of CdS and the performance of CdS/CdTe solar cells. *Sol. Energy Mater. Sol. Cells.* **67**, 297–304 (2001). [https://doi.org/10.1016/S0927-0248\(00\)00295-6](https://doi.org/10.1016/S0927-0248(00)00295-6)
- F. Taghizadeh Chari, M.R. Fadvieslam, Microstructural, optical and electrical properties of CdS thin films grown by spray pyrolysis technique as a function of substrate temperature. *Opt. Quant. Electron.* **51**, 377 (2019). <https://doi.org/10.1007/s11082-019-2081-8>
- T.L. Chu, S.S. Chu, Thin film II–VI photovoltaics. *Solid State Electron.* **38**, 533–549 (1995). [https://doi.org/10.1016/0038-1101\(94\)00203-R](https://doi.org/10.1016/0038-1101(94)00203-R)
- F. Rodríguez-Mas, J.C. Ferrer, J.L. Alonso, S. Fernández de Ávila, Expanded electroluminescence in high load CdS nanocrystals PVK-based LEDs. *Nanomaterials* **9**, 1212 (2019). <https://doi.org/10.3390/nano9091212>
- M.A. Buckingham, A.L. Catherall, M.S. Hill, A.L. Johnson, J.D. Parish, Aerosol-assisted chemical vapor deposition of CdS from xanthate single source precursors. *Cryst. Growth Des.* **17**, 907–912 (2017). <https://doi.org/10.1021/acs.cgd.6b01795>
- K. Senthil, D. Mangalaraj, S.K. Narayandass, Structural and optical properties of CdS thin films. *Appl. Surf. Sci.* **169–170**, 476–479 (2001). [https://doi.org/10.1016/S0169-4332\(00\)00732-7](https://doi.org/10.1016/S0169-4332(00)00732-7)
- P. Taneja, P. Vasa, P. Ayyub, Chemical passivation of sputter-deposited nanocrystalline CdS thin films. *Mater. Lett.* **54**, 343–347 (2002). [https://doi.org/10.1016/S0167-577X\(01\)00590-0](https://doi.org/10.1016/S0167-577X(01)00590-0)
- E.S. Yousef, A. El-Adawy, N. El Koshkhany, E.R. Shaaban, Optical and acoustic properties of TeO₂/WO₃ glasses with small amount of additive ZrO₂. *J. Phys. Chem. Solids* **67**, 1649–1655 (2006). <https://doi.org/10.1016/j.jpcs.2006.02.014>
- M. Baykul, A. Balcioglu, AFM and SEM studies of CdS thin films produced by an ultrasonic spray pyrolysis method. *Microelectron. Eng.* **51–52**, 703–713 (2000). [https://doi.org/10.1016/S0167-9317\(99\)00534-1](https://doi.org/10.1016/S0167-9317(99)00534-1)
- M. Tsuji, T. Aramoto, H. Ohyama, T. Hibino, K. Omura, Characterization of CdS thin-film in high efficient CdS/CdTe solar cells. *Jpn. J. Appl. Phys.* **39**, 3902–3906 (2000). <https://doi.org/10.1143/JJAP.39.3902>
- J. Nishino, S. Chatani, Y. Uotani, Y. Nosaka, Electrodeposition method for controlled formation of CdS films from aqueous solutions. *J. Electroanal. Chem.* **473**, 217–222 (1999). [https://doi.org/10.1016/S0022-0728\(99\)00250-8](https://doi.org/10.1016/S0022-0728(99)00250-8)
- R. Padmavathy, N. Rajesh, A. Arulchakkaravarthi, R. Gopalakrishnan, P. Santharaghavan, P. Ramasamy, Enhancement of photochemical deposition (PCD) and analysis of surface spread of CdS crystalline thin films. *Mater. Lett.* **53**, 321–325 (2002). [https://doi.org/10.1016/S0167-577X\(01\)00500-6](https://doi.org/10.1016/S0167-577X(01)00500-6)
- H.M. Rietveld, A profile refinement method for nuclear and magnetic structures. *J. Appl. Crystallogr.* **2**, 65–71 (1969). <https://doi.org/10.1107/S0021889869006558>
- R. A. Young, in *The Rietveld Method*, International Union Crystallography (Oxford University Press, Oxford, 1993)

20. R. Devi, P.K. Kalita, P. Purakayastha, B.K. Sarma, Growth and transport properties of nanocrystalline CdS thin film. *J. Optoelectron. Adv. Mater.* **10**, 3077–3082 (2008)
21. F. Chen, W. Jie, X. Cai, Effects of supersaturation on CdS film growth from dilute solutions on glass substrate in chemical bath deposition process. *Thin Solid Films* **516**, 2823–2828 (2008). <https://doi.org/10.1016/j.tsf.2007.04.167>
22. J. Ximello-Queibras, Physical properties of chemical bath deposited CdS thin films. *Sol. Energy Mater. Sol. Cells* **82**, 263–268 (2004). <https://doi.org/10.1016/j.solmat.2004.01.023>
23. B. Sankapal, R. Mane, C. Lokhande, Deposition of CdS thin films by the successive ionic layer adsorption and reaction (SILAR) method. *Mater. Res. Bull.* **35**, 177–184 (2000). [https://doi.org/10.1016/S0025-5408\(00\)00210-5](https://doi.org/10.1016/S0025-5408(00)00210-5)
24. A.L. Patterson, The Scherrer FORMULA for X-RAY PARTICLE SIZE determination. *Phys. Rev.* **56**, 978–982 (1939). <https://doi.org/10.1103/PhysRev.56.978>
25. O.A. Fouad, S.A. Makhlof, G.A.M. Ali, A.Y. El-Sayed, Cobalt/silica nanocomposite via thermal calcination-reduction of gel precursors. *Mater. Chem. Phys.* **128**, 70–76 (2011). <https://doi.org/10.1016/j.matchemphys.2011.02.072>
26. T.K. Pathak, V. Kumar, L.P. Purohit, H.C. Swart, R.E. Kroon, Substrate dependent structural, optical and electrical properties of ZnS thin films grown by RF sputtering. *Phys. E: Low-Dimens. Syst. Nanostruct.* **84**, 530–536 (2016). <https://doi.org/10.1016/j.physe.2016.06.020>
27. H. Fujiwara, *Spectroscopic ellipsometry: principles and applications*, Wiley (2007). <https://www.wiley.com/en-us/Spectroscopic+Ellipsometry%3A+Principles+and+Applications-p-9780470016084>
28. M. Alzaid, W.S. Mohamed, M. El-Hagary, E.R. Shaaban, N.M.A. Hadia, Optical properties upon ZnS film thickness in ZnS/ITO/glass multilayer films by ellipsometric and spectrophotometric investigations for solar cell and optoelectronic applications. *Opt. Mater. (Amst.)* **118**, 111228 (2021). <https://doi.org/10.1016/j.optmat.2021.111228>
29. M. Emam-Ismael, M. El-Hagary, E.R. Shaaban, S.H. Moustafa, G.M.A. Gad, Spectroscopic ellipsometry and morphological characterizations of nanocrystalline Hg_{1-x}MnxO oxide diluted magnetic semiconductor thin films. *Ceram. Int.* **45**(7), 8380–8387 (2019). <https://doi.org/10.1016/j.ceramint.2019.01.146>
30. E.R. Shaaban, M. El-Hagary, M. Emam-Ismael, A. Matar, I.S. Yahia, Spectroscopic ellipsometry and magneto-transport investigations of Mn-doped ZnO nanocrystalline films deposited by a non-vacuum sol-gel spin-coating method. *Mater. Sci. Eng. B* **178**, 183–189 (2013). <https://doi.org/10.1016/j.mseb.2012.11.005>
31. G.E. Jellison Jr., Spectroscopic ellipsometry data analysis: measured versus calculated quantities. *Thin Solid Films* **313–314**, 33–39 (1998). [https://doi.org/10.1016/S0040-6090\(97\)00765-7](https://doi.org/10.1016/S0040-6090(97)00765-7)
32. M. Zhao, R. Tong, X. Chen, T. Ma, J. Dai, J. Lian, J. Ye, Ellipsometric determination of anisotropic optical constants of single phase Ga₂O₃ thin films in its orthorhombic and monoclinic phases. *Opt. Mater. (Amst.)* **102**, 109807 (2020). <https://doi.org/10.1016/j.optmat.2020.109807>
33. M. Emam-Ismael, M. El-Hagary, H.M. El-Sherif, A.M. El-Naggar, M.M. El-Nahass, Spectroscopic ellipsometry and morphological studies of nanocrystalline NiO and NiO/ITO thin films deposited by e-beams technique. *Opt. Mater. (Amst.)* **112**, 110763 (2021). <https://doi.org/10.1016/j.optmat.2020.110763>
34. G.A. Niklasson, C.G. Granqvist, O. Hunderi, Effective medium models for the optical properties of inhomogeneous materials. *Appl. Opt.* **20**, 26 (1981). <https://doi.org/10.1364/AO.20.000026>
35. S. Tolansky, *Multiple-beam interference microscopy of metals* (Academic Press INC LTD, England, 1970)
36. K. Senthil, D. Mangalaraj, S. Narayandass, S. Adachi, Optical constants of vacuum-evaporated cadmium sulphide thin films measured by spectroscopic ellipsometry. *Mater. Sci. Eng. B* **78**, 53–58 (2000). [https://doi.org/10.1016/S0921-5107\(00\)00510-9](https://doi.org/10.1016/S0921-5107(00)00510-9)
37. X. Wu, F. Lai, L. Lin, J. Lv, B. Zhuang, Q. Yan, Z. Huang, Optical inhomogeneity of ZnS films deposited by thermal evaporation. *Appl. Surf. Sci.* **254**, 6455–6460 (2008). <https://doi.org/10.1016/j.apsusc.2008.04.023>
38. E.R. Shaaban, M. El-Hagary, M. Emam-Ismael, M.B. El-Den, Optical band gap, refractive index dispersion and single-oscillator parameters of amorphous Se₇₀S_{30-x}Sb_x semiconductor thin films. *Philos. Mag.* **91**, 1679–1692 (2011). <https://doi.org/10.1080/14786435.2010.544683>
39. P. Prathap, N. Revathi, Y.P. Venkata Subbaiah, K.T. Ramakrishna Reddy, Thickness effect on the microstructure, morphology and optoelectronic properties of ZnS films. *J. Phys. Condens. Matter.* **20**, 035205 (2008). <https://doi.org/10.1088/0953-8984/20/03/035205>
40. S. Mathew, K.P. Vijayakumar, Ellipsometric studies of microscopic surface roughness of CdS thin films. *Bull. Mater. Sci.* **17**, 421–427 (1994). <https://doi.org/10.1007/BF02745230>
41. S. Mathew, P.S. Mukerjee, K.P. Vijayakumar, Optical and surface properties of spray-pyrolysed CdS thin films. *Thin Solid Films* **254**, 278–284 (1995). [https://doi.org/10.1016/0040-6090\(94\)06257-L](https://doi.org/10.1016/0040-6090(94)06257-L)
42. J. Tauc, *Amorphous and liquid semiconductors* (Springer Science & Business Media, Berlin, 2012)

43. T.K. Tran, W. Park, W. Tong, M.M. Kyi, B.K. Wagner, C.J. Summers, Photoluminescence properties of ZnS epilayers. *J. Appl. Phys.* **81**, 2803–2809 (1997). <https://doi.org/10.1063/1.363937>
44. M.S. Bashar, R. Matin, M. Sultana, A. Siddika, M. Rahaman, M.A. Gafur, F. Ahmed, Effect of rapid thermal annealing on structural and optical properties of ZnS thin films fabricated by RF magnetron sputtering technique. *J. Theor. Appl. Phys.* **14**, 53–63 (2020). <https://doi.org/10.1007/s40094-019-00361-5>
45. V.H. Choudapur, S.B. Kapatkar, A.B. Raju, Structural and optoelectronic properties of zinc sulfide thin films synthesized by Co-precipitation method. *Acta Chem. Iasi* **27**, 287–302 (2019). <https://doi.org/10.2478/achi-2019-0018>
46. N. El-Kabnay, E.R. Shaaban, N. Afify, A.M. Abou-sehly, Optical and physical properties of different composition of $\text{In}_x\text{Se}_{1-x}$ thin films. *Phys. B Condens. Matter.* **403**, 31–36 (2008). <https://doi.org/10.1016/j.physb.2007.08.016>
47. O.L. Arenas, M.T.S. Nair, P.K. Nair, Chemical bath deposition of ZnS thin films and modification by air annealing. *Semicond. Sci. Technol.* **12**, 1323–1330 (1997). <https://doi.org/10.1088/0268-1242/12/10/022>
48. J. Lee, S. Lee, S. Cho, S. Kim, I.Y. Park, Y.D. Choi, Role of growth parameters on structural and optical properties of ZnS nanocluster thin films grown by solution growth technique. *Mater. Chem. Phys.* **77**, 254–260 (2003). [https://doi.org/10.1016/S0254-0584\(01\)00563-6](https://doi.org/10.1016/S0254-0584(01)00563-6)
49. A.E. Rakhshani, A.S. Al-Azab, Characterization of CdS films prepared by chemical-bath deposition. *J. Phys. Condens. Matter.* **12**, 8745–8755 (2000). <https://doi.org/10.1088/0953-8984/12/40/316>
50. S.A. Al Kuhaimi, Influence of preparation technique on the structural, optical and electrical properties of polycrystalline CdS films. *Vacuum* **51**, 349–355 (1998). [https://doi.org/10.1016/S0042-207X\(98\)00112-2](https://doi.org/10.1016/S0042-207X(98)00112-2)
51. O. Zelaya-Angel, J.J. Alvarado-Gil, R. Lozada-Morales, H. Vargas, A. Ferreira da Silva, Band-gap shift in CdS semiconductor by photoacoustic spectroscopy: evidence of a cubic to hexagonal lattice transition. *Appl. Phys. Lett.* **64**, 291–293 (1994). <https://doi.org/10.1063/1.111184>
52. K.L. Chopra, *Thin film phenomena* (Krieger Publishing Company, Krieger, 1979)
53. H. Oumous, H. Hadiri, Optical and electrical properties of annealed CdS thin films obtained from a chemical solution. *Thin Solid Films* **386**, 87–90 (2001). [https://doi.org/10.1016/S0040-6090\(00\)01767-3](https://doi.org/10.1016/S0040-6090(00)01767-3)
54. A. Segura, K. Wünnel, A. Chevy, Investigation of impurity levels in-type indium selenide by means of Hall effect and deep level transient spectroscopy. *Appl. Phys. A Solids Surf.* **31**, 139–145 (1983). <https://doi.org/10.1007/BF00624719>

Publisher's Note Springer Nature remains neutral with regard to jurisdictional claims in published maps and institutional affiliations.